Research Article | Vol. 11, No. 1 / 1 January 2021 / Optical Materials Express 35

Optical Materials EXPRESS

Electrical and optical properties linked to laser damage behavior in conductive thin film materials

MORTEN STEINECKE,[1,2,*] TANK ANKIT NARAN,[1,2] NILS CHRISTIAN KEPPLER,[3,4] PETER BEHRENS,[3,4] LARS JENSEN,[1,4] MARCO JUPÉ,[1,4] AND DETLEV RISTAU[1,4,5]

[1]*Laser Zentrum Hannover e.V., Laser Components Department, Hollerithallee 8, 30419 Hanover, Germany*
[2]*Leibniz University Hanover, Germany*
[3]*Institute for Inorganic Chemistry, Leibniz University Hanover, Callinstraße 9, 30165 Hanover, Germany*
[4]*Cluster of Excellence PhoenixD (Photonics, Optics, and Engineering–Innovation Across Disciplines), Hanover, Germany*
[5]*Institute of Quantum Optics, Leibniz University Hanover, Welfengarten 1,30167 Hanover, Germany*
[*]*m.steinecke@lzh.de*

Abstract: Epsilon-near-zero-materials (ENZ-materials) and their unique properties are key to the successful integration and miniaturization of optical components. Novel concepts, which promise significant progress in this field of research, such as optical switches and thin film electro-optical modulators, are possible when the electrical and optical properties of ENZ-materials are carefully exploited. To achieve a greater understanding of these properties, in this paper the electrical conductivity, optical transmittance, as well as absorption of thin indium tin oxide films, are investigated and linked to their laser-induced damage threshold in the ultra-short pulse regime. To the best of the authors' knowledge, this is the first concise study linking the electrical properties of indium tin oxide to its properties regarding high-power laser applications.

1. Introduction

Currently, a big effort is made for integration and size reduction of optical components. Of high interest for this is the availability of compact optical switching devices, both optically as well as electronically controlled. Epsilon-Near-Zero-materials, could play a key role in the development of these novel optical components [1]. The high interest in ENZ-materials is based on their different, extraordinary properties, such as their extreme nonlinear interactions [2]. Promising candidates for the realization of ENZ-materials are so called transparent conducting oxides [3]. In addition to their promising nonlinear properties, these materials allow, due to their inherent conductivity, the integration of electrical systems into optical components. Currently, the most widely used transparent conductive oxide is indium tin oxide (ITO). Its properties make it an established component in for example liquid-crystal-displays [4] and solar cells [5]. ITO features good conductivity and low absorption in the visible spectral range and can be manufactured by a variety of processes, such as spray pyrolysis [6], electron beam evaporation [7], both RF and DC magnetron sputtering [8–11] and ion beam sputtering (IBS) [12–14]. In addition to these promising features, ITO also exhibits extraordinary nonlinear properties [2,15]. For the implementation in high-end optical components, in addition to the desired electrical properties of the material, a precise knowledge of the optical properties such as the index of refraction and the extinction coefficient of the ITO-layers is necessary. In addition, at high laser powers the knowledge about the laser induced damage threshold (LIDT) is of major importance to avoid

#410081 https://doi.org/10.1364/OME.410081
Journal © 2021 Received 11 Sep 2020; revised 30 Oct 2020; accepted 2 Nov 2020; published 7 Dec 2020

Optical Materials EXPRESS

damaging of the produced components. Detailed studies already have been undertaken in the nanosecond pulse regime, investigating the dominant damage mechanisms and their mitigation, as well as the electrical and optical properties near the damage threshold. It was shown, that different deposition condition in magnetron processes can not only increase the LIDT, but also change the fundamental mechanisms involved [16–18]. For the utilization of the desired special nonlinear properties of ITO, high laser powers and consequently ultra short pulsed lasers are necessary. It is well-known that the damage mechanisms vary significantly for different temporal regimes of laser pulses [19]. Therefore, investigations about the laser induced damage in ITO for ultra short pulses are required.

The properties of ITO layers depend strongly on the manufacturing process and the post processing after deposition [20–22]. The aim of this paper is to provide an overview over the general behavior of ion beam sputtered ITO-layers with regards to their resistivity, index of refraction, extinction coefficient and LIDT. The manufacturing conditions were held constant, while the layers were annealed at different temperatures to achieve a variation in their properties.

2. Deposition process

To produce the ITO samples, an IBS-process was applied. The coating plant consists of a vacuum chamber the target material, in this case an indium-oxide/tin-oxide mixture (90 wt% indium-oxide and 10 wt% tin-oxide), an ion source and the substrate holder. In addition, an optical transmittance broadband monitor (BBM) was used to monitor the thickness during the coating.

The ion source used for this investigation is a commercial 16cm three grid source from *veeco* with the matching RF-neutralizer. A beam voltage of 1000V and a beam current of 250mA were chosen. The voltage of the accelerator grid was set to 300V. The chamber was evacuated to a base pressure of 1×10^{-3} Pa and argon (14sccm for the source and 6sccm for the neutralizer) as well as additional 9sccm of oxygen were added for sputtering and as process gas, respectively. The oxygen level is critical for the deposition if ITO layers, since it determines the initial (meaning before annealing or further processing) electrical and optical properties of the layers. From test runs with the described coating process, it was observed that 9sccm of oxygen produces layers with low resistivity and relatively high optical transmittance. Higher oxygen values would increase transmittance, but the resistivity would strongly increase, too. The pressure during sputtering is increased due to the process gases and measured to be approximately 2×10^{-2} Pa. The ITO was deposited as single layers with a thickness of approximately 315nm on fused silica substrates. To increase the number of samples available, two batches of samples were produced with identical parameters.

To change the properties of the ITO-layers, the samples were annealed after coating. The annealing was done in normal atmosphere in a temperature controlled oven. The samples were each heated up to the desired temperature and held there for 10h.

3. Characterization techniques

To characterize the samples for the relevant structural, optical and electrical properties, different measurement techniques were applied.

To investigate the physical structure of the layers, the samples analyzed with an optical microscope for each annealing step. To gain more details about the sample structure, also scanning electron microscopy (SEM) as well as x-ray diffraction (XRD) measurement were applied. The microscopic pictures were taken using an Carl Zeiss Axioscope optical microscope with differential interference contrast (DIC). The electron microscopy was done using an Quanta 400 FEG from Thermo Fisher Scientific Inc. (formerly FEI Company). The XRD measurements were performed with an Iso-Debyleflex 3003 (Stoe) between 20° and 70° 2θ with a step size of 0.05° 2θ and a measuring time of 2 s per step (40 kV, 30mA).

Optical Materials EXPRESS

A *Perkin Elmer L19* spectralphotometer was used for transmittance measurements before and after annealing of each sample. The measurements were then evaluated for the index of refraction n and the extinction coefficient k using the commercially available software *OptiLayer* and its characterization module *OptiChar* [23]. The refractive index was fitted applying a Sellmeier-model and the extinction coefficient was fitted using tabulated data. An example of the transmittance measurements and the fit with OptiChar is presented in Fig. 1(a) and (b). Since the determination of k from transmittance measurements is subject to relatively high uncertainty for small losses, additionally laser calorimetric absorption measurements according to ISO11551 were performed [24]. The samples were irradiated by a cw laser at a wavelength of 1064nm and the sample temperature was monitored to determine absolute absorption. A more detailed explanation of the measurement procedure can be found in [25].

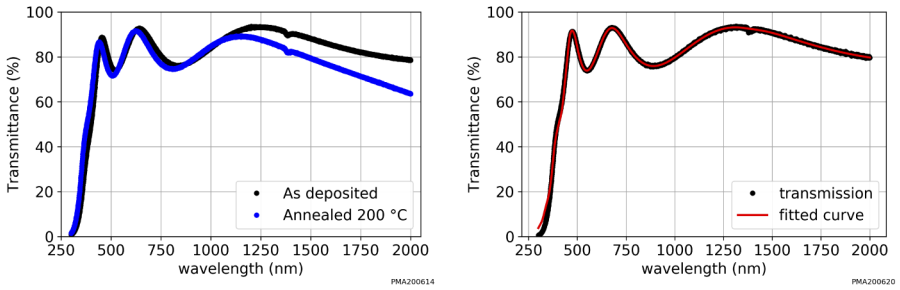

(a) (b)

Fig. 1. (a) Exemplary transmittance curves for annealed and as-deposited ITO single layers. The transmittance was fitted using commercially available software, the resulting fit is presented in (b).

Besides the basic optical properties, the electronic properties are of particular interest in ENZ-materials. Especially the conductivity/resistivity is of interest for electrical applications. To reliably determine the resistance of the manufactured layers, a four-terminal sensing method was applied [26]. The surface of the samples was contacted using spring-loaded, gold plated pins. The pins are brought into contact with the surface in reproducible position and a *Rigol DM3058E* digital multimeter was used to do the four terminal sensing. Since each pair of the four pins was equidistant during the measurement, and the thickness of the layer is much smaller than its lateral dimension as well as the distance between the pins, the sheet resistance $R_\square$ can be calculated as follows [27]:

$$R_\square = \frac{\pi}{\ln(2)} R \tag{1}$$

Where R is the resistance measured with the digital multimeter. Since the thickness d is well known from the optical transmittance measurements, the material resistivity ρ can be calculated:

$$\rho = d \cdot R_\square = d \frac{\pi}{\ln(2)} R \tag{2}$$

Finally, for the application in high-performance optical systems, also the laser induced damage is of great interest. To determine the usability of the produced samples regarding this property, the LIDT of the samples was measured in their different annealing states. The LIDT measurements were performed utilizing a *Coherent Monaco* femtosecond laser system. The laser wavelength was 1035nm, the pulse duration was 250fs for the investigation of annealing effects and varied from 250fs to 1000fs for the investigation of the influence of pulse duration. The effective beam diameter was 66 μm. A repetition rate of 10kHz was chosen and the measurements were

Optical Materials EXPRESS

performed according to ISO21254-2 [28], following an 200,000-on-1 procedure with detection of scattered laser radiation as damage criterion during the measurements. The repetition rate and number of pulses was chosen to achieve similar conditions to what is expected in later applications. The setup is schematically presented in Fig. 2(a). Each sample was irradiated at 126 sites, and the state of each site was verified by optical Nomarski microscopy after irradiation. Figure 2(b) shows a few, exemplary damaged spots. From the damage statistics of the different sites, the lifetime LIDT H_∞ was calculated as value for comparison between the samples [28]. In addition to the investigation of the LIDT in relation to the annealing temperature, the convenient adjustment of the pulse duration on the utilized laser system also allowed to measure the dependence of the LIDT on pulse duration.

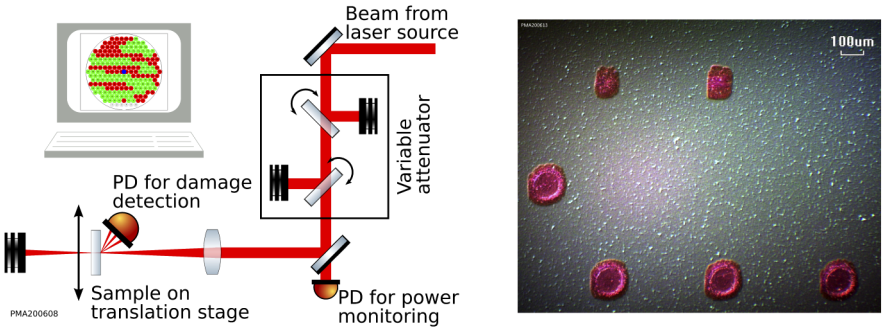

Fig. 2. Schematical representation of the setup for LIDT measurements (a) and a microscopic picture of several destroyed spots after the LIDT test (b).

4. Results and discussion

The characterization techniques described in section 3 allow the measurement of the different properties with regards to the annealing temperature.

4.1. Structural investigations

To investigate the change in the structure of the samples caused by the post-process annealing, different characterization techniques described in section 3 were applied.

Investigations with the optical DIC-microscopy allow a first insight into the changes, especially of the optical properties, in the material caused by annealing. Pictures of samples annealed at four different temperatures are presented in Fig. 3. After coating, each layer shows a "clean" surface, e.g. no particles or structure are visible. The layers stay this way up to an annealing temperature of 200°C. At higher temperatures, the annealing initiates the formation of small, black dots, which is visible in Fig. 3(b) for an annealing temperature of 250°C. At 275°C, the black dots seem to have expanded in a roughly circular shape, covering most of the sample surface. At higher temperatures, the sample surface is completely covered by the expanded areas and the boundaries between the different zones can be observed. Similar changes in the structure of ITO-films have been observed, albeit at different temperatures [29,30] and were linked to crystallization in the material.

It has to be noted, that colors are, due to the nature of the differential interference contrast, somewhat arbitrary, and in addition, have been adjusted for optimal visibility of the features. Therefore, black color does not imply optical losses or opaqueness. The samples were, independently of annealing temperature, transparent to the naked eye and did not show significant scattering.

Optical Materials EXPRESS

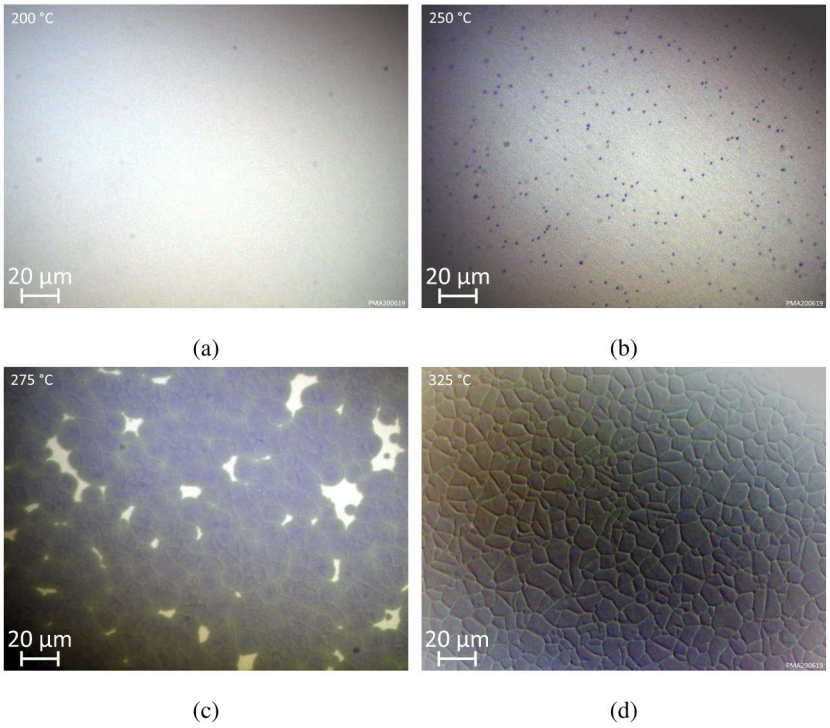

Fig. 3. DIC-Microscopic analysis of ITO-samples annealed at different temperatures. (a) shows the layer after annealing at 200°C, without any significant features. Annealing at 250°C produces small black dots (b), and annealing at 275°C causes further growth of the black dots (c). At 325°C the sample surface is completely covered (d).

To investigate the crystallization effects in more detail, XRD-measurements were taken for samples annealed at different temperatures. The results are presented in Fig. 4. The figure clearly illustrates the mainly amorphous nature of the ITO-layers up to a temperature of 250°C. It has to be noted, that the detection of sub-micrometer crystalline grains with XRD-measurements is limited, when their density in an amorphous material is small. Consequently, the initial crystallization phase with crystal seeds in only small quantity may not be visible in this measurement, which might explain the small dots visible in Fig. 3(b), which do not show in the XRD-measurements. For 275°C and higher temperatures, the samples show a crystalline structure typical for ITO with a low amount of tin-doping [31]. This matches the observations from the optical microscopy, where a clear difference between the samples at 250°C and 275°C can be observed.

Because neither the optical microscopy or the XRD-measurements truly show the micro structure of the layer, an additional SEM-analysis was performed. The resulting pictures show a smooth surface without features. Especially the inital phase of the crystallization, which is visible in Fig. 3(b) with the small, dark dots, was not visible in the electron microscope. The only change to the layer structure was observed at higher temperatures, where the sample surface is cracked, which is shown in Fig. 5. The pictured sample was annealed at 325°C. Taking the microscopic picture from Fig. 3(d) into account, it is reasonable to assume that the cracks happened at the boundaries of the crystalline zones.

Optical Materials EXPRESS

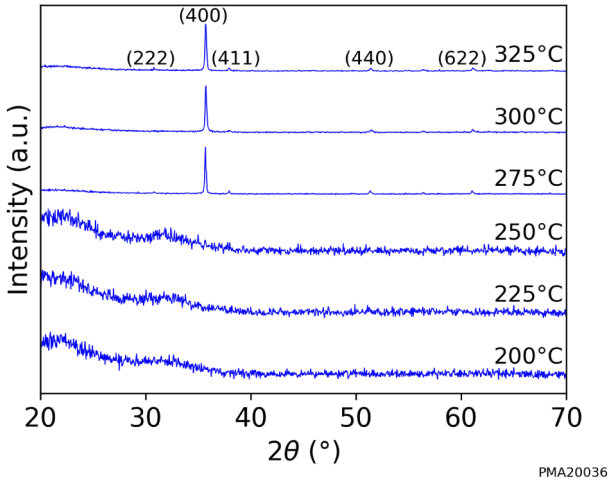

Fig. 4. XRD-measurements taken for samples annealed at different temperatures. From 250°C to 275°C a clear transition from an amorphous structure to a crystalline one is observed.

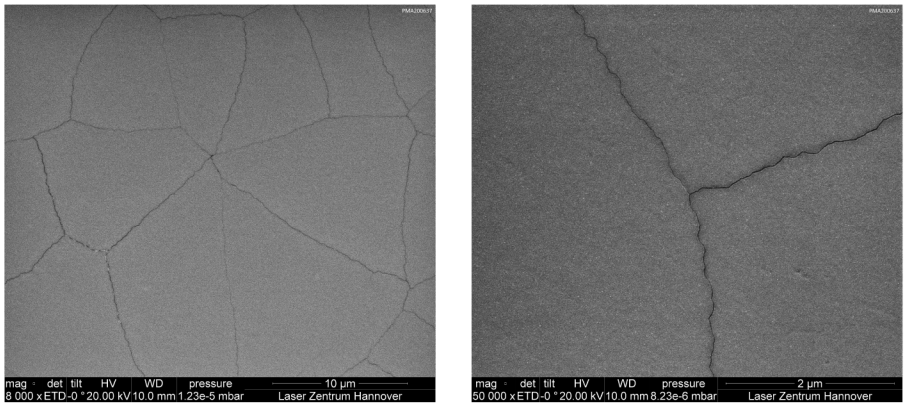

(a) (b)

Fig. 5. Cracking after annealing at higher temperatures which is observed in the ITO-layers. (a) gives an overview over the size of the flakes while (b) shows the cracks in more detail.

4.2. Index of refraction and extinction coefficient

The index of refraction and the extinction coefficient are the most significant parameters when implementing optical materials into optical coatings. The measurements were performed according to the procedure described in section 3 and the results are presented in Fig. 6. The two properties show a significant variation depending on the annealing temperature. The refractive index at 1035nm increases from approximately 1.94 directly after deposition to almost 2 at 200°C. At higher temperatures, the index of refraction decreases again, to approximately 1.92 at 325°C.

The extinction coefficient at 1035nm decreases from a value of roughly 6×10^{-3} to 5×10^{-4} when annealed at 200°C. Treated at higher temperatures, the extinction rises to a local maximum of approximately 1×10^{-2} at 275°C, and decreases again for 300°C and 325°C.

To achieve greater insight into the material properties and reduce the uncertainty for the measurement of the extinction coefficient, additionally also laser calorimetric measurements

Optical Materials EXPRESS

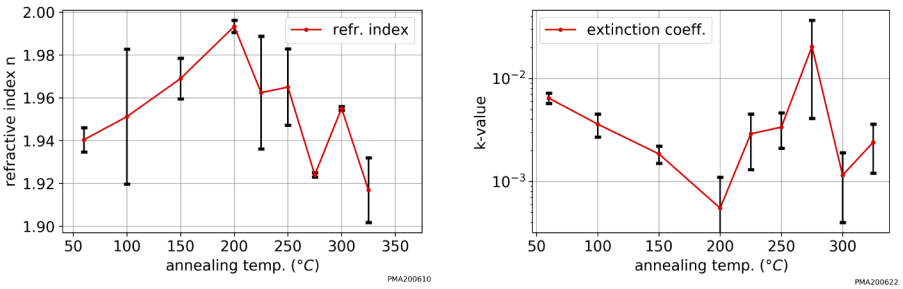

(a) (b)

Fig. 6. Refractive index and k-value for the annealed ITO-layers. The values are presented for a wavelength of 1035nm.

of the absorption were performed according to the procedure described in section 3. For better comparability with the extinction coefficients calculated from the spectral transmittance measurements, the equivalent k-values were calculated from the absolute absorption values. The results are presented in Fig. 7. The absorption behaves quite similar to the extinction coefficient determined by the spectralphotometric measurement and reproduces the minimum at 200°C as well as the local maximum at 275°C. It has to be noted however, that there is a significant quantitative mismatch for samples that were not annealed, as well as samples annealed at 275°C and 325°C. The reason for this mismatch is related to the measurement accuracy of both procedures.

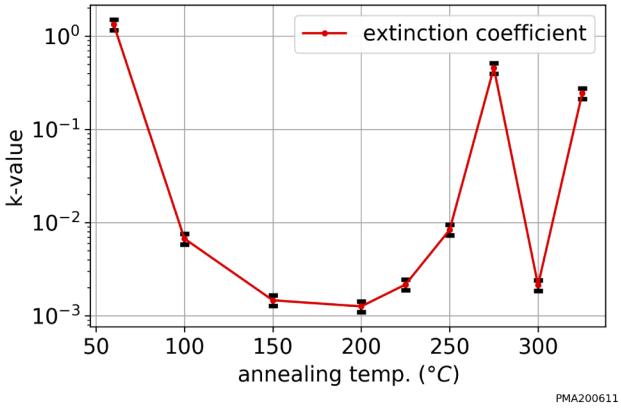

Fig. 7. The absorption values determined by laser calorimetry at 1064nm. For better comparability, the equivalent extinction coefficient was calculated from the absolute absorption values.

Overall, the curves show a consistent behaviour: An increase in refractive index corresponds with decreasing optical losses for annealing temperatures up to 200°C. At higher temperatures, the losses increase and the refractive index decreases again. The changes in the optical properties seem to correlate with the changes observed in the structure of the annealed layers. Up to 200°C, the layer structure is not affected by the annealing and the optical properties improve. This is interpreted as a filling of oxygen vacancies during the annealing, which was performed under ambient atmosphere. The filling of oxygen vacancies would reduce free carrier density and therefore would reduce the optical losses. The worsening at temperatures higher than 200°C

Optical Materials EXPRESS

could result from newly generated free carriers. This behavior can be understood in more detail, when the electrical properties discussed in section 4.3 are taken into account.

4.3. Electrical resistivity

The electrical resistivity of the samples was measured with the technique described in section 3 for each of the different annealing temperatures. The resulting values are plotted in Fig. 8. The samples have a relatively low resistivity directly after coating (since the coating temperature is approximately 60°C, this is the starting temperature). The resistivity increases for the samples with higher annealing temperatures up until 250°C. At temperatures of 275°C, the resistivity drops almost down to its original value and then again rises rapidly at higher temperatures.

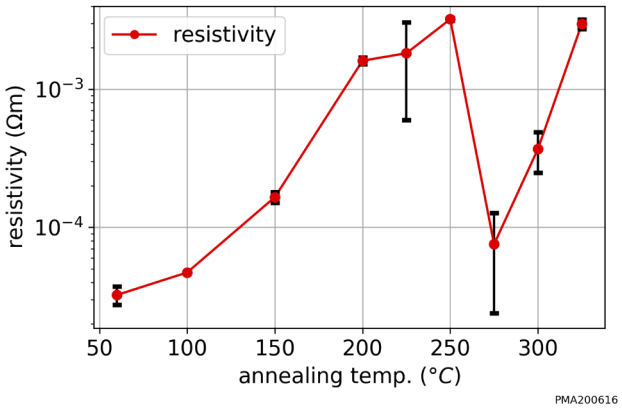

Fig. 8. The resulting electrical resistivities after annealing.

The behavior of the resistivity can be understood, when the two contribution mechanism for electrical conductivity in ITO are considered. The free carriers and therefore the electrical conductivity in ITO mainly result from doubly charged oxygen vacancies and the integration of four-valent Sn-atoms [32]. It has been shown, that in the case of amorphous ITO, the Sn-atoms do not contribute to the free carriers [33]. So below the initialization of crystalline seeds at approximately 200°C, only the oxygen vacancies are contributing to the conductivity of the samples. Since the annealing was done under ambient atmosphere, it is assumed that the observed rise of resistivity is caused by filling of the initially present oxygen vacancies. This reduces the free carrier density until the initialization temperature is reached. Above 200°C sub-micrometer crystal grains are created. This is indicated by the microscopic investigations. Obviously, the optical properties are significantly changed in this temperature range. As described in section 4.2, above 200°C, the optical losses increase and the index of refraction decreases. This can be clearly correlated to a smaller growth of the resistivity at these temperatures. With respect to the microscopic pictures shown in Fig. 3, it can be assumed that the creation of sub-micrometer crystals leads to an increase of free carriers by activation of the Sn^{4+}-states [34]. With increasing size of the crystal grains, the active tin-doping strongly increases which causes a significant drop in resistivity, which can be observed in Fig. 8 in the transition from 250°C to 275°C. The increasing resistivity for higher annealing temperatures is assumed to result in small part from the continued filling of oxygen vacancies, but mainly from the cracking of the layers observed in Fig. 5.

4.4. LIDT

The laser induced damage threshold of the ITO layers is a critical parameter for the application in high power optical systems. The LIDT was determined according to the procedure described

Optical Materials EXPRESS

in section 3 and the results are presented in Fig. 9 and Table 1. The damage threshold of the manufactured samples directly after coating is measured to be 1.4 J cm^{-2}, and can be increased by annealing at 200°C to approximately 2.7 J cm^{-2}. Annealing at higher temperatures lowers the LIDT to a minimum of 1.2 J cm^{-2} at 300°C. Figure 10 shows damage morphologies resulting from the different annealing temperatures for a pulse duration of 250fs. Directly after deposition and for temperatures of up to 250°C, the damage morphology is characteristic for the damages in the ultra-short pulse regime. The transition from 250°C to 275°C causes a clear change in the damage morphology, which hints at thermal effects taking part in the damage process at 275°C. At higher temperatures, the morphology returns to the initial, typical state. The dominating role thermal effects play in forming laser damages at nanosecond pulse durations in ITO is well known [16–18]. In the femtosecond regime investigated here, the expected behavior is different and thermal effects should play almost no role [19].

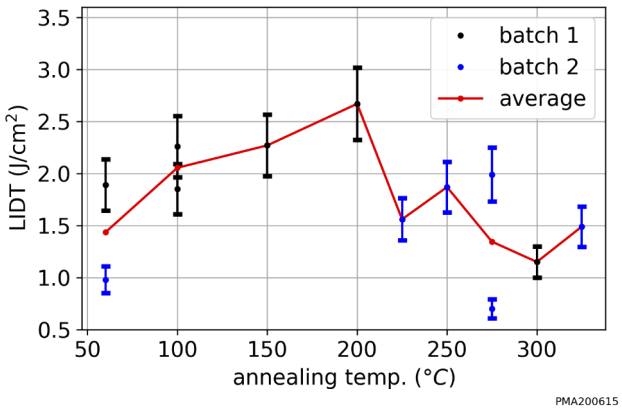

Fig. 9. LIDT-values for the samples after annealing at different temperatures.

Table 1. LIDT-values for the samples after annealing at different temperatures.

Temperature (°C)	60	100	150	200	225	250	275	300	325
LIDT batch 1 (J cm^{-2})	1.9	1.9 / 2.3	2.3	2.7	-	-	-	1.2	-
LIDT batch 2 (J cm^{-2})	1	-	-	-	1.6	1.9	2 / 0.7	-	1.5

These measurements agree with what was already observed in sections 4.2 and 4.3. The behavior of the LIDT can similarly be related to the previous measurements. It can be assumed, that the LIDT correlates negatively with the free carrier density, meaning that high carrier densities lead to lower LIDTs. From the measurements of optical losses, it can be derived, that the non-treated samples have a high density of free carriers. Consequently, the measured damage threshold is low. Treatment at higher temperatures leads to reduction of the free carriers, and consequently to an increase in LIDT. With the generation of additional carriers from the activation of Sn^{4+}-states, the LIDT decreases again.

In addition to testing the influence of the annealing process on the LIDT, also the influence of the pulse duration was tested for two different annealing temperatures, to compare the behaviour to that of a standard, dielectric material. The resulting curves are presented in Fig. 11. It can be observed, that the LIDT exhibits a local minimum at 600fs and 800fs, respectively. This is very unexpected. From experience, for a dielectric material the LIDT's dependence on the pulse duration is defined by the *Mero-Rudolph-rule*, where the LIDT H is given by [35]:

$$H = (c_1 + c_2 E_g)\tau_p^{\kappa} \tag{3}$$

Optical Materials EXPRESS

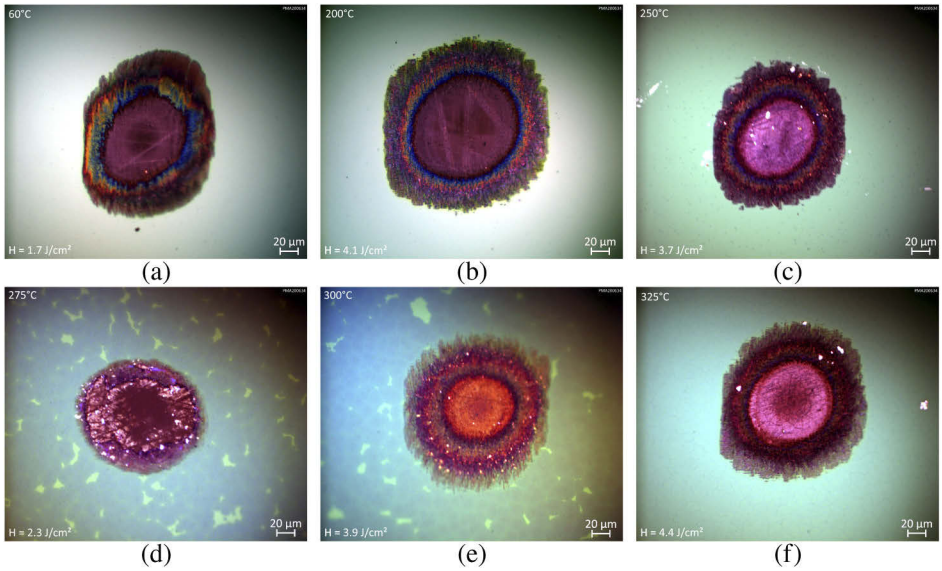

Fig. 10. The damage morphologies at 250fs resulting from the different annealing temperatures. The temperature is 60°C for (a), 200°C for (b), 250°C for (c), 275°C for (d), 300°C for (e) and 325°C for (f). A clear change of the morphology due to crystallization effects in the material can be observed at 275°C.

Where c_1, c_2 as well as κ are material and pulse independent parameters ($c_1 = -0.16 \pm 0.02$ J cm^{-2}, $c_2 = 0.074 \pm 0.004$ J cm^{-2} and $\kappa = 0.30 \pm 0.03$) from [35]. Since this particular relation is only valid at laser wavelengths of 800nm and for single-pulse destruction, a correction factor has to be added to account for the changed laser wavelength λ and the applied S-on-1-procedure:

$$H = (c_1 + c_2 E_g)\tau_p^{\kappa} \cdot r(S, \lambda) \tag{4}$$

Consequently, for fixed laser wavelengths and pulse number S, the only variable parameters for calculating the LIDT are the band gap energy E_g and the pulse duration τ_p. For each of the tested samples, the band gap should be constant, so that the LIDT is proportional to $\tau_p^{0.3}$. Consequently,

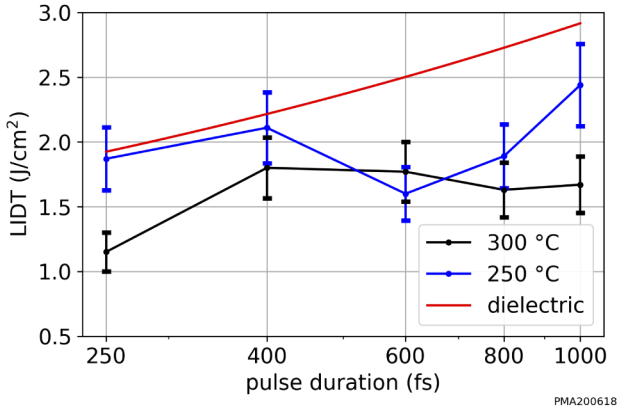

Fig. 11. Measured LIDT-values of two different ITO-layers for different pulse durations. The behavior expected for a dielectric material is indicated by the red curve.

Optical Materials EXPRESS

the LIDT for a normal dielectric material should show a monotonic increase with increasing pulse durations. This is also illustrated in Fig. 11.

It can be observed, that the curves for the two ITO-samples significantly deviate from that of a dielectric material. The LIDTs are much lower than what is expected from the *Mero-Rudolph-rule* Since it was shown, that in both crystalline and amorphous ITO, free carriers are present, it can be assumed that the resonance of the free carriers takes part in the damage behavior.

5. Conclusion

In summary, it can be observed that the fundamental structure and the derived optical and electrical properties of ITO can be varied in a significant range by annealing of deposited layers. The results indicate, that depending on the intended application of the material, the treatment of the samples has to be chosen carefully. With respect to the structural properties, the results indicate two fundamentally different states of the material, which can be tuned by temperature treatment. The measurements performed in this work show a clear correlation between a model assumption and the experimental results. The samples were characterized applying optical DIC-microscopy, XRD-analysis, SEM-imaging, spectrophotometric transmission measurements, laser calorimetric absorption measurements and determination of the ultra short pulse LIDT.

Directly after IBS-coating, the layers are amorphous in structure and oxygen vacancies in the material provide a high density of free carriers, leading to low resistivity (measured down to 3×10^{-5} Ωm) and high optical losses. The tin doping does not seem to impact the material properties in this amorphous state. Annealing under ambient atmosphere leads to filling of the oxygen vacancies and therefore lower densities of free carriers, lower optical losses and high resistivities. Upwards of annealing temperatures of 200°C, the material starts to form sub-micrometer crystal grains which continue to grow with higher temperature in our experiment. This crystallization process can be observed using a combination of optical microscopy and XRD-analysis. In this crystalline structure, the Sn^{4+}-states are activated and provide additional free carriers, which in turn improves electrical resistivity and increases optical losses.

The LIDT behaves in close correspondence with the optical properties and losses. It exhibits a maximum value of approximately 2.7 J cm^{-2} correlating with the lowest optical absorption. This indicates that the carrier density varies with different temperature treatments since the LIDT strongly depends on free carriers.

These results show, that depending on the intended application, the deposition- and post-processing parameters have to be carefully considered. Especially the annealing temperature allows great influence over the structure of the ITO-layers and the derived optical properties, electrical resistivity as well as laser power handling capabilities.

Funding

Bundesministerium für Wirtschaft und Energie (03THW05K12); Niedersächsisches Ministerium für Wissenschaft und Kultur; Deutsche Forschungsgemeinschaft (EXC 2122, Project ID 390833453).

Acknowledgments

The authors would like to thank Gina-Madeleine Haase for the support with the laser calorimetric measurements and Dr. Tatjana Melnyk for supporting the SEM-analysis.

The authors like to thank *Coherent Inc.* for providing the laser source.

Disclosures

The authors declare no conflicts of interest.

Optical Materials EXPRESS

References

1. N. Kinsey, C. DeVault, A. Boltasseva, and V. M. Shalaev, "Near-zero-index materials for photonics," Nat. Rev. Mater. **4**(12), 742–760 (2019).
2. M. Z. Alam, I. D. Leon, and R. W. Boyd, "Large optical nonlinearity of indium tin oxide in its epsilon-near-zero region," Science **352**(6287), 795–797 (2016).
3. U. Koch, C. Hoessbacher, J. Niegemann, C. Hafner, and J. Leuthold, "Digital plasmonic absorption modulator exploiting epsilon-near-zero in transparent conducting oxides," IEEE Photonics J. **8**(1), 1–13 (2016).
4. X. Yan, F. W. Mont, D. J. Poxson, M. F. Schubert, J. K. Kim, J. Cho, and E. F. Schubert, "Refractive-index-matched indium–tin-oxide electrodes for liquid crystal displays," Jpn. J. Appl. Phys. **48**(12), 120203 (2009).
5. Z. Tan, W. Zhang, Z. Zhang, D. Qian, Y. Huang, J. Hou, and Y. Li, "High-performance inverted polymer solar cells with solution-processed titanium chelate as electron-collecting layer on ITO electrode," Adv. Mater. **24**(11), 1476–1481 (2012).
6. V. Vasu and A. Subrahmanyam, "Reaction kinetics of the formation of indium tin oxide films grown by spray pyrolysis," Thin Solid Films **193-194**, 696–703 (1990).
7. I. Hamberg, C. Granqvist, K.-F. Berggren, B. Sernelius, and L. Engström, "Optical properties of transparent and infra-red-reflecting ITO films in the 0.2–50 μm range," Vacuum **35**(6), 207–209 (1985).
8. G. Sberveglieri, S. Groppelli, and G. Coccoli, "Radio frequency magnetron sputtering growth and characterization of indium-tin oxide (ITO) thin films for NO2 gas sensors," Sens. Actuators **15**(3), 235–242 (1988).
9. A. P. Amalathas and M. M. Alkaisi, "Effects of film thickness and sputtering power on properties of ITO thin films deposited by RF magnetron sputtering without oxygen," J. Mater. Sci.: Mater. Electron. **27**(10), 11064–11071 (2016).
10. E. Kusano, J. Kawaguchi, and K. Enjouji, "Thermal stability of heat-reflective films consisting of oxide–ag–oxide deposited by dc magnetron sputtering," J. Vac. Sci. Technol., A **4**(6), 2907–2910 (1986).
11. C. David, B. Tinkham, P. Prunici, and A. Panckow, "Highly conductive and transparent ITO films deposited at low temperatures by pulsed DC magnetron sputtering from ceramic and metallic rotary targets," Surf. Coat. Technol. **314**, 113–117 (2017).
12. J. C. C. Fan, "Preparation of sn-doped In_2O_3 (ITO) films at low deposition temperatures by ion-beam sputtering," Appl. Phys. Lett. **34**(8), 515–517 (1979).
13. Y. Zhang, P. Cheng, K. Yu, X. Zhao, and G. Ding, "ITO film prepared by ion beam sputtering and its application in high-temperature thermocouple," Vacuum **146**, 31–34 (2017).
14. G. E. Henein, J. Topolancik, and K. Siebein, "High quality oxide films deposited at room temperature by ion beam sputtering," MRS Adv. **3**(4), 219–224 (2018).
15. M. Steinecke, T. Kellermann, M. Jupé, L. O. Jensen, and D. Ristau, "Measurement setup for the determination of the nonlinear refractive index of thin films with high nonlinearity," in *Laser-Induced Damage in Optical Materials 2018: 50th Anniversary Conference*, V. E. Gruzdev, D. Ristau, M. Soileau, G. J. Exarhos, and C. W. Carr, eds. (SPIE, 2018).
16. J.-H. Yoo, M. G. Menor, J. J. Adams, R. N. Raman, J. R. I. Lee, T. Y. Olson, N. Shen, J. Suh, S. G. Demos, J. Bude, and S. Elhadj, "Laser damage mechanisms in conductive widegap semiconductor films," Opt. Express **24**(16), 17616 (2016).
17. J.-H. Yoo, M. Matthews, P. Ramsey, A. C. Barrios, A. Carter, A. Lange, J. Bude, and S. Elhadj, "Thermally ruggedized ITO transparent electrode films for high power optoelectronics," Opt. Express **25**(21), 25533 (2017).
18. J.-H. Yoo, A. Lange, J. Bude, and S. Elhadj, "Optical and electrical properties of indium tin oxide films near their laser damage threshold," Opt. Mater. Express **7**(3), 817 (2017).
19. D. Ristau, ed., *Laser-Induced Damage in Optical Materials* (CRC Press, 2014).
20. M. Boehme and C. Charton, "Properties of ITO on PET film in dependence on the coating conditions and thermal processing," Surf. Coat. Technol. **200**(1-4), 932–935 (2005).
21. J. Lian, D. Zhang, R. Hong, P. Qiu, T. Lv, and D. Zhang, "Defect-induced tunable permittivity of epsilon-near-zero in indium tin oxide thin films," Nanomaterials **8**(11), 922 (2018).
22. T. Sathiaraj, "Effect of annealing on the structural, optical and electrical properties of ITO films by RF sputtering under low vacuum level," Microelectron. J. **39**(12), 1444–1451 (2008).
23. A. V. Tikhonravov and M. K. Trubetskov, "Optilayer software," Software. OptiLayer GmbH, Watzmannring 71, 85748 Garching b. München.
24. L. Jensen, I. Balasa, K. Starke, and D. Ristau, "Spectrally resolved laser calorimetric absorptance measurements," in *Laser-Induced Damage in Optical Materials: 2007*, G. J. Exarhos, A. H. Guenther, K. L. Lewis, D. Ristau, M. J. Soileau, and C. J. Stolz, eds. (SPIE, 2007).
25. U. Willamowski, D. Ristau, and E. Welsch, "Measuring the absolute absorptance of optical laser components," Appl. Opt. **37**(36), 8362–8370 (1998).
26. M. B. Heaney, "Electrical conductivity and resistivity," in *Measurement, Instrumentation, and Sensors Handbook*, (CRC Press, 2014).
27. L. Valdes, "Resistivity measurements on germanium for transistors," Proc. IRE **42**(2), 420–427 (1954).
28. ISO, *ISO 21254-2:2011, Lasers and Laser-related Equipment — Test Methods for Laser-induced Damage Threshold — Part 2: Threshold Determination* (International Organization for Standardization, 2011).
29. E. Nishimura, M. Ando, K. ichi Onisawa, M. Takabatake, and T. Minemura, "Structural change during annealing of amorphous indium-tin oxide films deposited by sputtering with H_2O addition," Jpn. J. Appl. Phys. **35**(Part 1, No. 5A), 2788–2792 (1996).

Optical Materials EXPRESS

30. N. M. Ahmed, F. A. Sabah, H. Abdulgafour, A. Alsadig, A. Sulieman, and M. Alkhoaryef, "The effect of post annealing temperature on grain size of indium-tin-oxide for optical and electrical properties improvement," Results Phys. **13**, 102159 (2019).
31. M. Thirumoorthi and J. T. J. Prakash, "Structure, optical and electrical properties of indium tin oxide ultra thin films prepared by jet nebulizer spray pyrolysis technique," J. Asian Ceram. Soc. **4**(1), 124–132 (2016).
32. T. J. Vink, M. H. F. Overwijk, and W. Walrave, "The active dopant concentration in ion implanted indium tin oxide thin films," J. Appl. Phys. **80**(7), 3734–3738 (1996).
33. J. R. Bellingham, W. A. Phillips, and C. J. Adkins, "Electrical and optical properties of amorphous indium oxide," J. Phys.: Condens. Matter **2**(28), 6207–6221 (1990).
34. H.-C. Lee and O. O. Park, "Behaviors of carrier concentrations and mobilities in indium–tin oxide thin films by DC magnetron sputtering at various oxygen flow rates," Vacuum **77**(1), 69–77 (2004).
35. M. Mero, J. Liu, W. Rudolph, and K. Starke, "Scaling laws of femtosecond laser pulse induced breakdown in oxide films," Phys. Rev. B **71**(11), 115109 (2005).